# Deterioration Mechanisms of Ultra-High-Performance Concrete Under Various Sulfuric Acid and Sulfate Attack Conditions

Galal Fares[1] · Yassir M. Abbas[1] · Mohammad Iqbal Khan[1]

## Abstract

The formulation of ultra-high-performance concrete necessitates the use of a high cement content. The alkaline nature of cement makes it susceptible to acid attacks. In addition, its high $C_3A$ content causes its vulnerability to sulfate attack under the development of expansive ettringite, where porosity plays an important role. The main objective of this study was to figure out how mass loss and dimensional instability affected the rate of reaction and its relationship to acid concentration. It is noted that in contrast to sulfuric acid attack, sulfate attack on ultra-high-performance concrete (UHPC) is characterized by the accumulation of sulfate ions near the surface until reaching a critical concentration known as the threshold value. However, the reaction effect was not remarkable, as attributed to the extremely low porosity. The effect of curing was found to have a minimal influence on acid resistivity because it is a kind of spontaneous acid-base reaction that cannot be alleviated. In this research work, the UHPC's service life can be predicted when exposed to different concentrations of sulfuric acid. When comparing acid and sulfate attacks, the latter becomes negligible. Despite the use of silica fume and fly ash, the reactivity with sulfuric acid was found to occur spontaneously and rely on cement content and acid concentration. A concentration of 2.5% sulfuric acid is the threshold concentration after which a substantial change in the development of strength takes place. Both reactions were monitored on different types of samples over time using several techniques, such as XRD, TGA, and DSC and optical microscopy.

**Keywords** Ultra-high-performance concrete (UHPC) · Sulfuric acid attack · Sulfate attack · Mass loss · Volumetric stability

## 1 Introduction

### 1.1 Background

Concrete has a wide range of applications in everyday life. Because of the high cost and vulnerability of metal pipes to chemical transportation, chemicals are transported around the world through concrete pipelines. However, the chemical resistance of concrete varies according to the nature of the reactivity of the chemicals and the type of chemical interaction. Additionally, because concrete is naturally alkaline, it is very vulnerable to acid reactions [1].

In most cases, coatings and sealants formulated to resist chemicals are applied to concrete and metal pipes and structures [2–4]. It is important to note, however, that the cost, effectiveness, and durability of the coatings are influenced by many parameters and conditions, as the uniform coating along the pipes and units may not always be ideal [5]. The surface of metal and concrete pipes is frequently coated with highly chemical-resistant coatings. In infrastructural construction, uniform coating is not always possible, so coated products are limited by their cost, efficiency, and durability due to a variety of factors and conditions. In comparison to metal, concrete construction is more cost-effective.

Mixtures of concrete can be classified into several types and classes. These categories include types such as normal, high-strength, high-performance, and ultra-high-performance concrete, whose cement content varies from low in normal concrete to high in ultra-high-performance concrete (UHPC). Predictably, UHPC will become more susceptible to acid attacks because of its high cement content [6, 7]. It is reported that acid resistance does not rely on concrete

✉ Mohammad Iqbal Khan
miqbal@ksu.edu.sa

1 Department of Civil Engineering, College of Engineering, King Saud University, P.O. Box 800, 11421 Riyadh, Saudi Arabia

strength but rather relies on capillary porosity, which should be reduced to the maximum value [8]. The authors believe that the chemical reaction will be initiated once hydrated and unhydrated cement particles are brought into contact with an acid solution, liberating calcium and other ions and forming gypsum and ettringite in a series of damaging chemical reactions. Society is affected directly by the durability of the sanitary safety of the sewage system, which is directly affected by concrete durability. The long-term durability of sewage systems is an essential aspect of environmental protection and the sanitary safety of society. The acid resistivity of conventional and ultra-high-performance concrete in sewage systems was discussed and parameters such as pH and acid consumption were defined [9]. The concrete damage is reported to depend on the degree of acid saturation near the surface. On the other hand, the neutrality of sodium sulfate solution has a great effect on the mechanism of the reaction where the sulfate ions accumulate near the surface and react with the aluminate phase to form ettringite, which leads to the deterioration of the cementitious matrix.

There is inconsistent evidence in the literature concerning the effects of supplementary cementitious materials (SCMs) on the acidity resistance of cementitious systems [10, 11]. In industrial operations, sulfuric acid, the most aggressive type, is used in the manufacturing process. Sulfuric acid can also be produced by acid rain, initiated by $SO_2$ air pollution, flowing through pipes and sewage systems and causing steel corrosion and concrete deterioration [12–15]. A sewage system and other wastewater sources can contain biogenic acids and artificial sulfuric acids. Different species of bacteria, such as chemolithotrophic bacteria, phototrophic bacteria, and chemoorganotrophic bacteria, produce biogenic acids. There is worldwide concern over the corrosion of concrete sewer pipes brought on by sulfuric acid attacks.

## 1.2 Significance, Objectives, and Scope of the Study

In different studies [16–19], the impact of sulfate attacks on normal and high-performance concrete has been investigated. However, there are limited studies of sulfate attacks on UHPC. In the current investigation, we have investigated the time-dependent effects of various dosages (1.25, 2.5, 5, and 10% vol.) of sulfuric acid (SA) on the compressive strength as well as the mass and volume stability of UHPC.

It is feasible to avoid the crucial reduction of acid concentration to the level where the reaction rates are altered from linear to exponential, which indicates a threshold value. Few experiments and simulations have looked at the relevant factors that control chemical corrosion, such as curing age and the presence or absence of micro-steel fibers. The main objective of this study was to investigate the effect of sulfuric acid and sodium sulfate solutions on the UHPC blend developed from dune sand. A second aim was to model the

**Table 1** Chemical analysis of fine powders

| Oxides (%) | PC | FA | SF |
|---|---|---|---|
| $SiO_2$ | 20.41 | 55.23 | 86.20 |
| $Al_2O_3$ | 5.32 | 25.95 | 0.49 |
| $Fe_2O_3$ | 4.1 | 10.17 | 3.79 |
| CaO | 64.14 | 1.32 | 2.19 |
| MgO | 0.71 | 0.31 | 1.31 |
| $SO_3$ | 2.44 | 0.18 | 0.74 |
| $TiO_2$ | 0.30 | – | – |
| $Na_2Oeq$ | 0.1 | 0.86 | 2.80 |
| L.O.I | 2.18 | 5 | 2.48 |

impact of the elevated sulfuric acid (a high level of sulfuric acid concentration beyond standard or typical conditions) concentration over a short time period until half of the mass is lost and beyond. Moreover, the effect of incorporating micro-steel fibers on expansion and mass loss over time was assessed. The impact of aggressive curing, namely curing in aggressive media such as sulfuric acid solutions, was evaluated, as was the mineralogical change, through a stereo-optical microscope, X-ray diffraction (XRD), and thermal analysis. The proposed model identifies mass and volume changes as the key parameters for predicting the service life of the UHPC unit. It accounts for the rate of cementitious matrix dissolution in the UHPC mix.

In this research, the impacts of aggressive curing on the investigated samples were evaluated for mechanical degradation and mineralogical change using XRD analysis, a stereo-optical microscope, and thermal analysis. Further, the proposed model identified mass and volume changes as the key parameters for predicting the service life of the UHPC unit. It accounted for the rate of cementitious matrix dissolution in the UHPC mix. Here, the evaluation of the UHPC mix was conducted in a 10% $Na_2SO_4$ solution under sulfate attack (SS). Moreover, the expansion of UHPC bars was studied in solutions containing 10% SA and 10% SS. The volume of the sulfuric acid solution was between 10 and 30 times that of the sample. Moreover, this study was dedicated to evaluating the rate of dimension change of UHPC mix taking place in the sewerage system in a way that can simulate the damage and estimate its rate.

## 2 Experimental Program

### 2.1 Materials

In this investigation, we utilized type I ordinary Portland cement (OPC) as the principal binder, adhering to ASTM

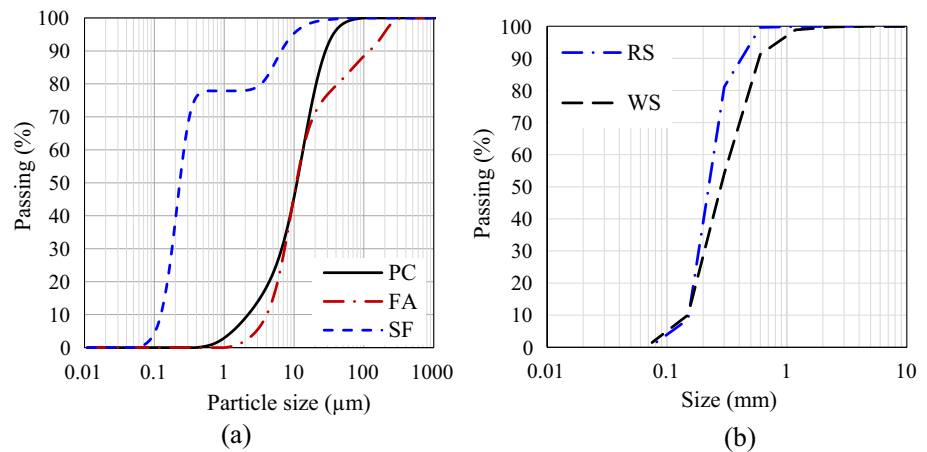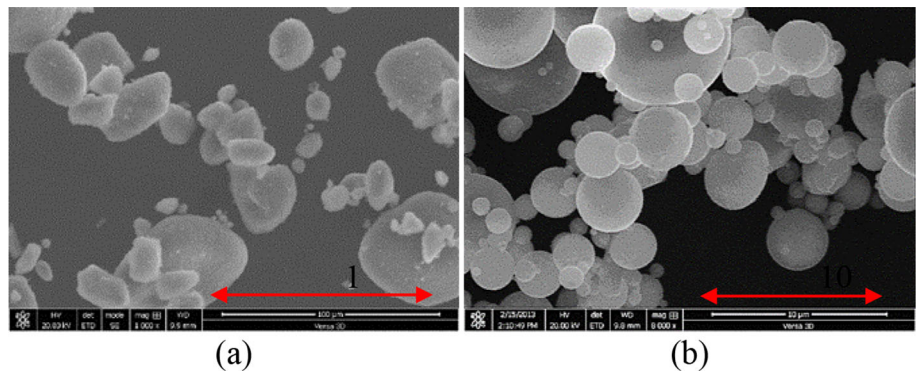**Fig. 1** PSD analysis of **a** fine powders, and **b** aggregates



(a)　　　　　　　　　　　　　　　　　(b)

**Fig. 2** Photomicrograph of SF and FA: **a** Condensed SF (1000x) and **b** FA (8000x)



(a)　　　　　　　　　　　　　　　　　(b)

C150 [20] specifications. Supplementary cementitious materials, namely silica fume (SF) and class F fly ash (FA), were incorporated to augment the overall composition. The Axios Max X-ray fluorescence (XRF) machine facilitated the determination of the fine powders' chemical composition, as meticulously detailed in Table 1. Furthermore, the particle size distribution (PSD) of both fine powders and aggregates underwent thorough examination, as depicted in Fig. 1 (a) and (b), respectively, utilizing a laser diffraction particle size analyzer (LA-950). Specific gravities of PC, FA, and SF were measured at 3.15, 2.7, and 2.2, respectively. Notably, a Versa 3D dual-beam field emission scanning electron microscope (SEM) was employed for a comprehensive microstructural investigation, with Fig. 2 showcasing SEM photomicrographs of fine powders. The incorporation of a hybrid system of micro-steel fibers (T1, T2, and T3) in the UHPC mix is elucidated, and Table 2 provides an in-depth exploration of the physicomechanical parameters of all fibers (Fig. 3).

In the pursuit of UHPC mix development, fine desert aggregates sourced from the Arabian Peninsula, specifically identified as red dune and white sands (RS and WS), played a pivotal role in this study. Under saturated surface dry conditions (SSD), the specific gravities of RS and WS

**Table 2** Physical properties of micro-steel fibers

| Micro-steel Type (T) | T1 | T2 | T3 |
|---|---|---|---|
| Aspect ratio | 65 | 100 | 150 |
| Length (mm) | 13 | 20 | 30 |
| Diameter ($\mu$m) | 200 | 200 | 200 |
| Density (g/cm$^3$) | 7.85 | 7.85 | 7.85 |
| Tensile strength (MPa) | | | 2300–2600 |

were determined to be 2.65 and 2.74, respectively. Photomicrographs of RS and WS, captured using a stereo-optical microscope, along with elemental SEM–EDX analyses, are presented in Fig. 4, offering a visual understanding of the aggregates' composition. To complement this, Table 3 and Fig. 4 meticulously detail the physical properties and sieve analysis of fine aggregates, adhering to the standards set by ASTM C128 [21], respectively.

Furthermore, in the formulation of the UHPC mixture, we employed a polycarboxylic ether-based (PCE) superplasticizer characterized by a solid content of approximately 0.36% and a specific gravity of 1.1. The PCE dosage calculation was determined as a percentage of its solid content

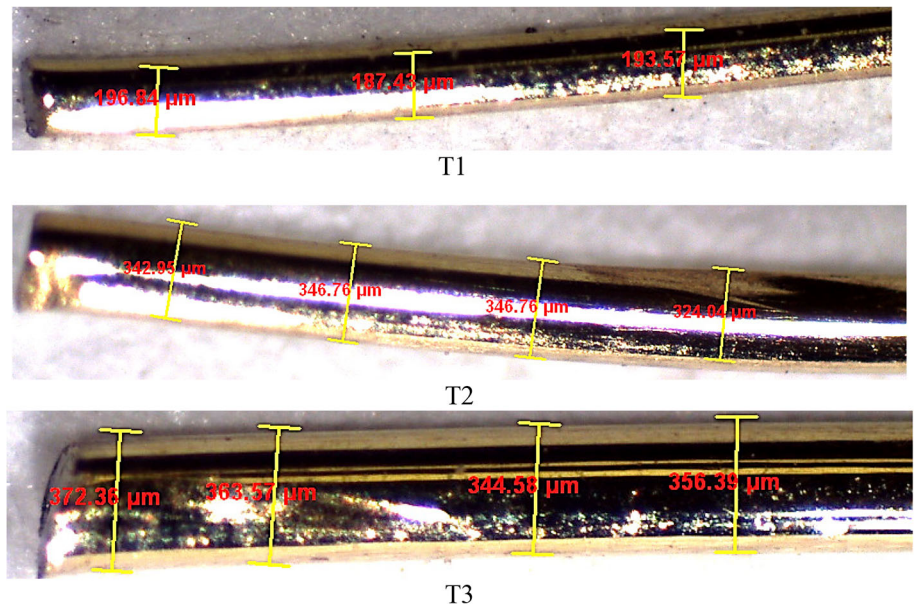**Fig. 3** Measurement of micro-steel fiber diameters of different steel size groups (T-T3)



T1

T2

T3

**Fig. 4** Microscopic analysis of fine aggregates using **a** RS and **b** WS with a magnification of 35x
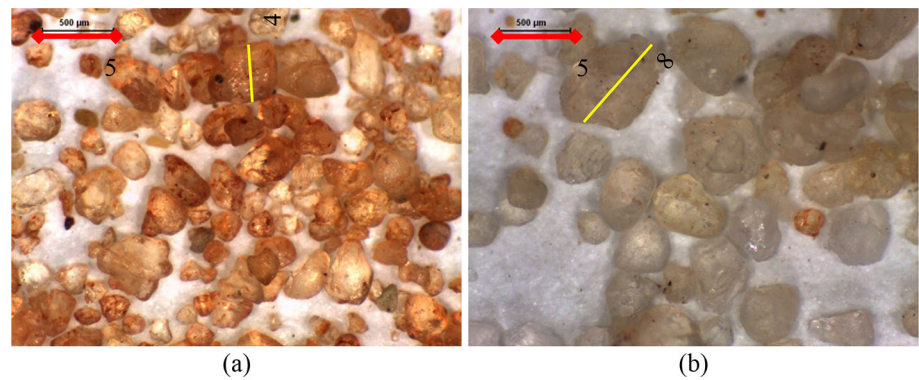


(a)                    (b)

**Table 3** Physical properties of procured local fine aggregates

| Physical properties | RS | WS |
|---|---|---|
| Bulk Specific Gravity (OD Basis) | 2.64 | 2.73 |
| Bulk Specific Gravity (SSD Basis) | 2.65 | 2.74 |
| Apparent Specific Gravity | 2.67 | 2.76 |
| Absorption, % | 0.30 | 0.37 |
| Fineness modulus (range of 2.3–3.1) | 1.11 | 1.46 |

relative to the weight of the total binder content. Additionally, we underscore the significance of selecting the optimal aggregate combination of DS and WS, known for achieving the best packing density [22, 23]. This deliberate choice is reflected in the development of the UHPC mix composition, meticulously outlined in Table 4.

## 2.2 Methods

### 2.2.1 Mixing, Casting, and Testing

The incorporation of a high-shear mixer, exemplified by MischTechnik's UEZ ZZ 50-S boasting a 95-L capacity (UEZ Mischtechnik GmbH, Stuttgart, Germany), stands as a critical factor in achieving a successful UHPC mix. The

**Table 4** Mix proportions of the developed UHPC (in kg/m$^3$)

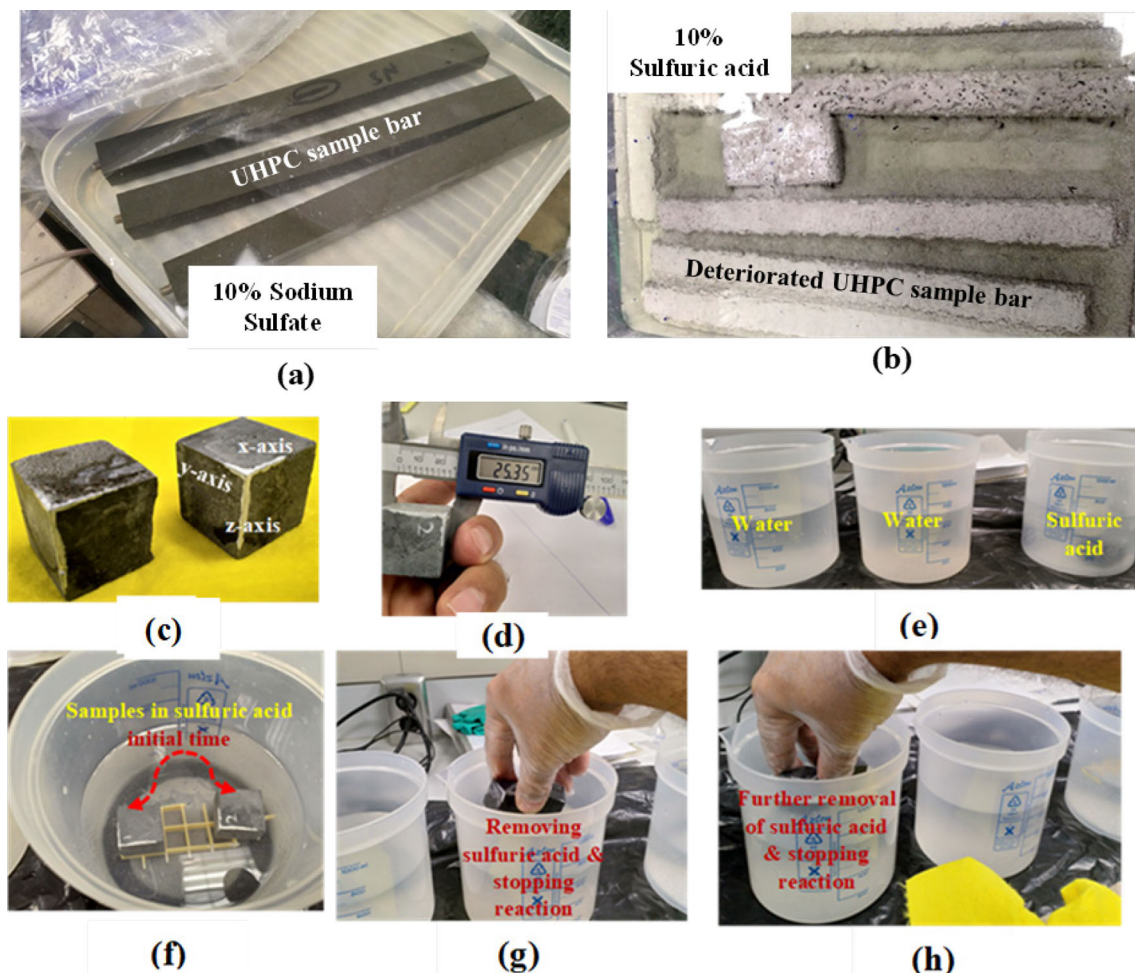| PC | SF | FA | WS | RS | Water | SP | Fiber | | |
|---|---|---|---|---|---|---|---|---|---|
| | | | | | | | T1 | T2 | T3 |
| 1138.7 | 242.4 | 67.0 | 487.9 | 163.2 | 215.7 | 40.3 | 153.9 | 43.6 | 7.7 |

**Fig. 5** Bar sample expansion in **a** 10% sodium sulfate solution and **b** 10% sulfuric acid, as well as **c** adding reference lines to the test cubes, **d** taking initial measurements, **e** plastic containers with water to stop reaction and 10% sulfuric acid solution, **f** initial time for samples in sulfuric acid, **g** taking samples out of sulfuric acid solution, **h** immersion in water to remove acid and stop the reaction during measurement, and **c-h** this test setup postpones linearity deviation time (LDT)

meticulous mixing sequence, akin to various other concrete mixing processes, initiates with the high-speed homogenization of all dry solid materials for 5 min. Subsequently, the second step involves the addition of a superplasticizer to the mixing water, including absorption water, facilitating homogenization under high-speed mixing until the desired flowability is attained. The final step in this process involves the introduction of fibers, meticulously added at medium speed, culminating in a comprehensive UHPC mixture. The subsequent phase entails casting samples into molds of varying sizes for prisms (40 × 40 × 160 mm and 20 × 20 × 280 mm) and cubes (50 × 50 × 50 mm and 25 × 25 × 25 mm). These samples are then subjected to a 24-h curing period under controlled laboratory conditions (21 ± 2°C temperature and 100% relative humidity).

### 2.2.2 Compressive Strength Test

In the absence of fibers, the compressive strength testing of cube samples was conducted after exposure to various curing regimes, utilizing the Model Instron (3000 kN capacity) universal machine. The testing protocol maintained a constant loading rate of 0.2 MPa/s, ensuring uniformity in the evaluation process. The preference for cubes over cylinders in this context is underscored, attributed to the ease of testing without necessitating specialized grinding and preparation techniques, as required for cylinders [24]. Notably, the strength of the cubic samples has been systematically monitored over time, offering valuable insights into their performance under diverse environmental conditions, including normal, sulfate, and sulfuric acid media.
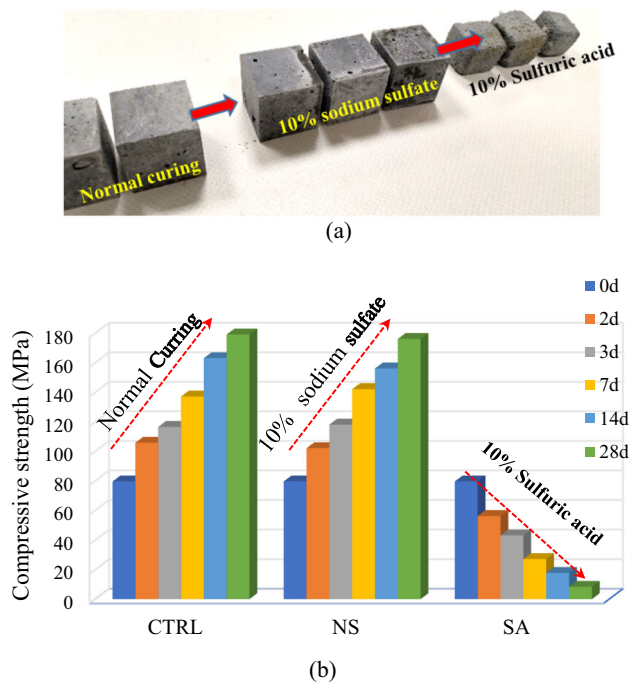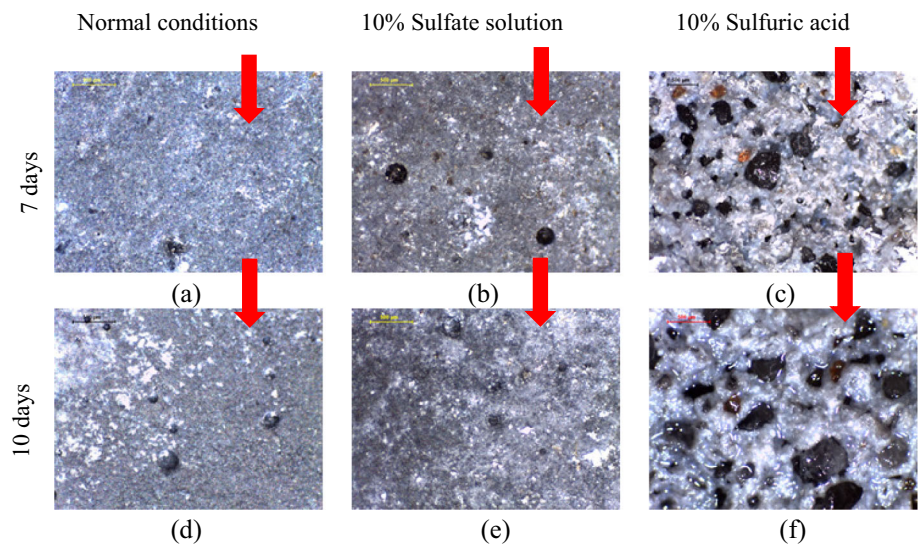
(a)



(b)

**Fig. 6** Effect of different media **a** water, 10% sodium sulfate, and 10% sulfuric acid on the stability of UHPC cubes for compressive strength, as well as **b** the effect of different media of normal curing (CTRL), 10% sodium sulfate (NS), and 10% sulfuric acid (SA) on the compressive strength

### 2.2.4 Sulfate and Sulfuric Acid Attacks

The high cement content in the UHPC mix renders it particularly susceptible to acid attacks, particularly sulfuric acid attacks. To comprehensively assess the impact of varying sulfuric acid concentrations (1.25, 2.5, 5, and 10%), a series of tests was conducted to evaluate their effect on mass. A trial test revealed that 10% sulfuric acid represents the maximum concentration capable of inducing extreme damage within a shorter timeframe, aligning with findings from prior investigations [25]. Subsequently, a 10% sodium sulfate solution was prepared to examine its influence on the strength of cubes and the expansion of UHPC bars. Adhering to ASTM 1012 [26], the testing solution's volume should be 3.5 times the overall volume of the tested samples. However, in an effort to expedite the simulation of reactions within a condensed timeframe, a testing solution volume 30 times that of the tested samples was also prepared, specifically for estimating the linearity deviation time (LDT), as illustrated in Fig. 5. The rates of mass and volume change were meticulously measured over the initial minutes, hours, and days. To comprehensively evaluate the effects of sulfuric acid and sodium sulfate solutions, two sample sizes were prepared—cubes (25 mm) and bars (25 × 25 × 285 mm), enabling a thorough analysis of the impact on different dimensions of the UHPC specimens.

## 3 Experimental Results and Discussion

### 3.1 Compressive Strength

The UHPC cubes immersed in normal curing conditions as well as 10% sodium sulfate and 10% sulfuric acid solutions were investigated for compressive strength at various
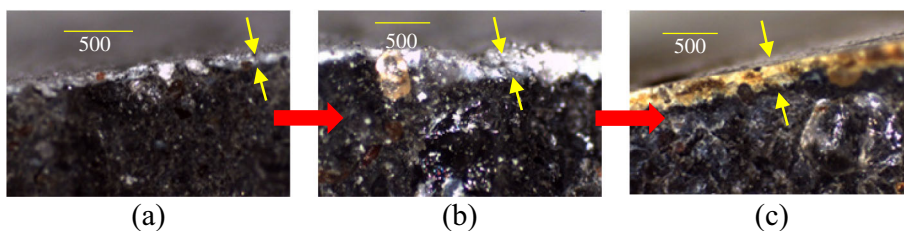
### 2.2.3 Microscopic Analysis

The current study employs an optical microscope as a testing technique, chosen for its ease and simultaneous nature. Specifically, the surface alteration of test samples submerged in various solutions of sulfate and sulfuric acids was meticulously observed using a Leica stereomicroscope, model EZ4HD.

**Fig. 7** Optical microscopic examination of UHPC cubes immersed in **a** normal conditions, **b** 10% sodium sulfate solution, and **c** 10% sulfuric acid solution at 7 days and the corresponding 10 days, as in (**d**), (**e**) and (**f**), respectively

**Fig. 8** Optical microscopic examination of UHPC cubes immersed in 10% sulfuric acid shows **a** initial reaction **b** further reaction and **c** formation of the weak sulfur-rich layer
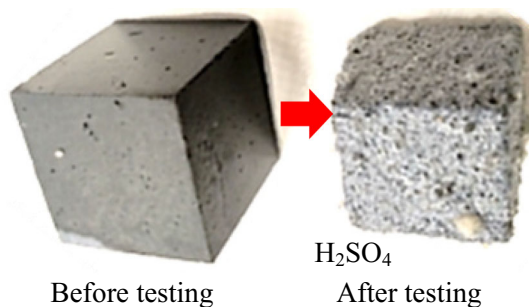


**Fig. 9** Effect of sulfuric acid attack on concrete morphology (by the authors)



**Fig. 10** Expansion measurement of UHPC samples immersed in 10% -Na$_2$SO$_4$ solution over time of two samples (S1 and S2)



**Fig. 11** Expansion measurement of UHPC samples immersed in 10% sulfuric acid solution over time of two samples (S1 and S2)

ages. The absence of micro-steel fibers was necessary to account for the interaction between the cementitious matrix and chemicals without adding another dimension to fibers' corrosion reaction with chemicals. The typical effect of different curing conditions is depicted in Fig. 6a. The cubes immersed in 10% sulfuric acid are greatly affected and eroded compared to those in normal conditions and 10% sodium sulfate. Both conditions are also used to simulate severe sewerage systems and similar conditions. In this experiment, the proportion of the chemical medium volume to the volume of the samples was determined to be 10. The results of the strength development are shown in Fig. 6b. This figure demonstrated that the compressive strengths of the samples immersed in 10% sulfuric acid have significantly declined, while the tested samples cured in normal conditions and 10% sodium sulfate have steadily increased over time. From the figure, it can be concluded that the penetration of sulfate ions into the UHPC matrix is delayed by the low permeability and neutrality of the solution, as shown by normal conditions and 10% sodium sulfate. However, there is a slight reduction in strength due to the effect of the accumulation of sulfate ions over time. The acidic nature of sulfuric acid accelerates the erosion of the alkaline cementitious matrix and sulfate attack.

## 3.2 Microscopic Analysis

In this part of the study, the surface modification that takes place under the effects of different curing conditions is p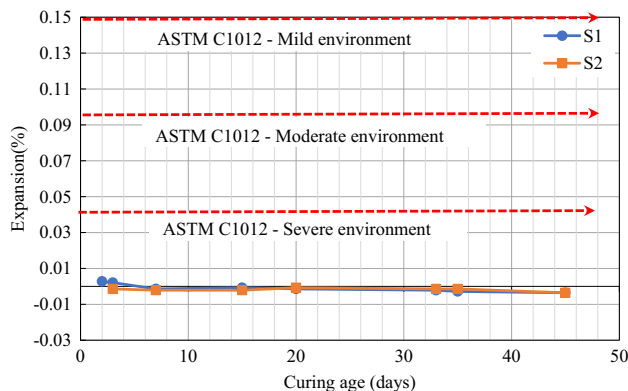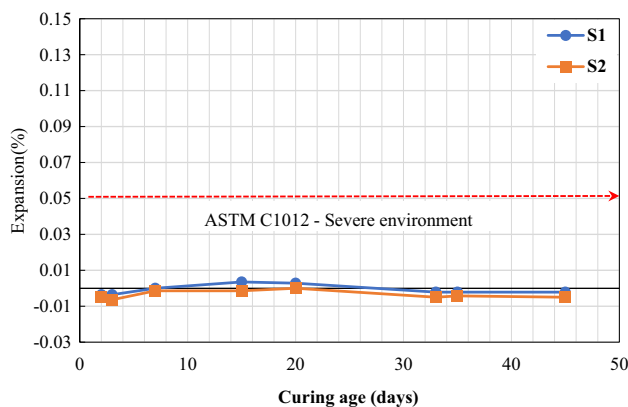resented. No surface modifications have been noted in the samples cured under normal conditions or in a 10% sulfate solution. It is reported that the penetration of sulfate ions into the UHPC matrix is nearly negligible due to the high degree of impermeability [27]. However, the spontaneous reaction of the UHPC cement paste with acid leads to surface erosion of the cementitious matrix that exacerbates over time, and the exposure of the sand grains increases over time as well. It becomes a mere acid-base reaction of low activation energy; it is a spontaneous reaction that accelerates with the concentration of the reactant. Figure 7 shows the microscopically

**Fig. 12** Interaction between UHPC bars and 10% sulfuric acid after **a** 1 day and **b** 28 days, where the dissolution process appears **c** initially on bars, **d** over time with **e** sulfur-rich layer formation, and how bars deteriorated **f** initially and after **g** long time
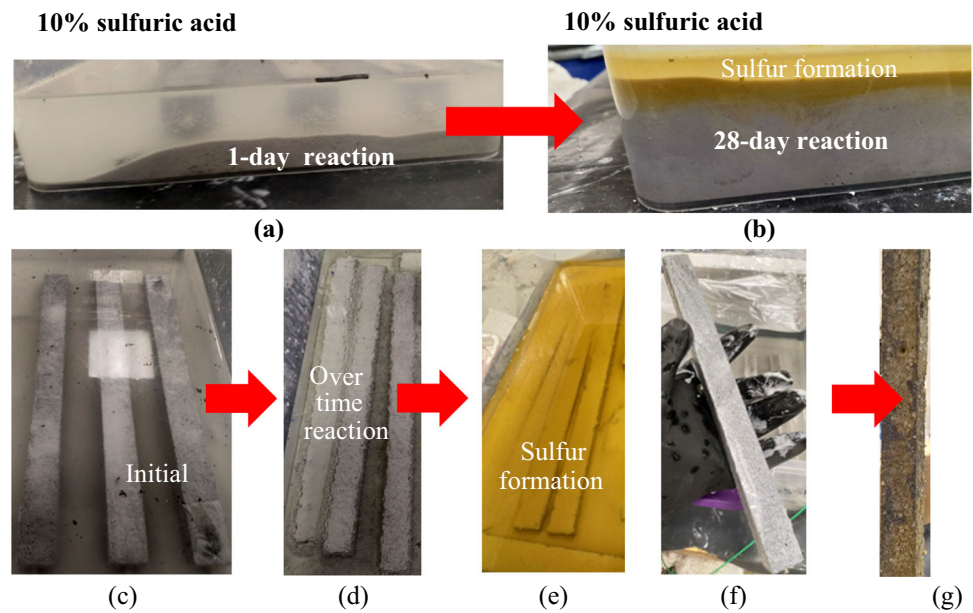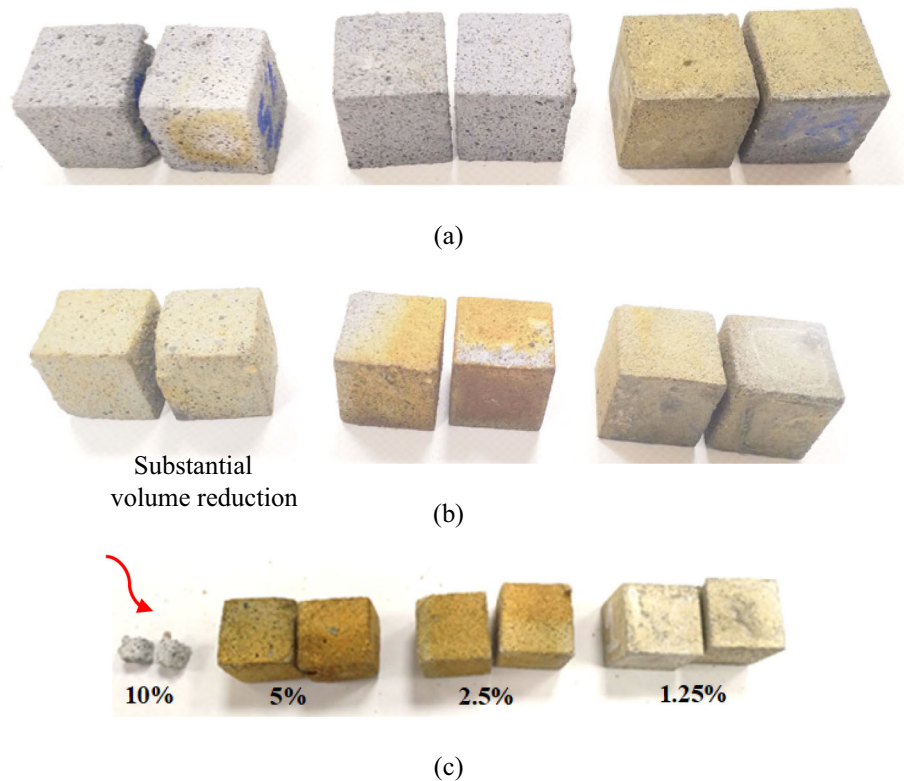


**Fig. 13** Effect of different concentrations of sulfuric acid on UHPC samples at **a** 7 days, **b** 14 days, and **c** 28 days



analyzed samples cured in normal (water-cured) and aggressive media. Additionally, Fig. 8 illustrates the progress of the chemical attack by sulfuric acid and the mechanism of degradation. The surface reaction was triggered by the dissolution reaction of cement phases at high pH [Eqs. (3)–(5)] and the formation of gypsum and a sulfur-rich weak bonding phase (Fig. 8 (a)–(b)). The reaction continues with the formation of a critical thickness, resulting in the detachment and loss of this layer, together with mass loss due to the dissolution of the cement phase, as demonstrated in Fig. 8(c).

## 3.3 Sulfate and Sulfuric Acid Attacks

Sulfate attack is classified as internal and external. Sulfate-carrying compounds react with $C_3A$ in cement to form ettringite, which is expansive and leads to local expansion.
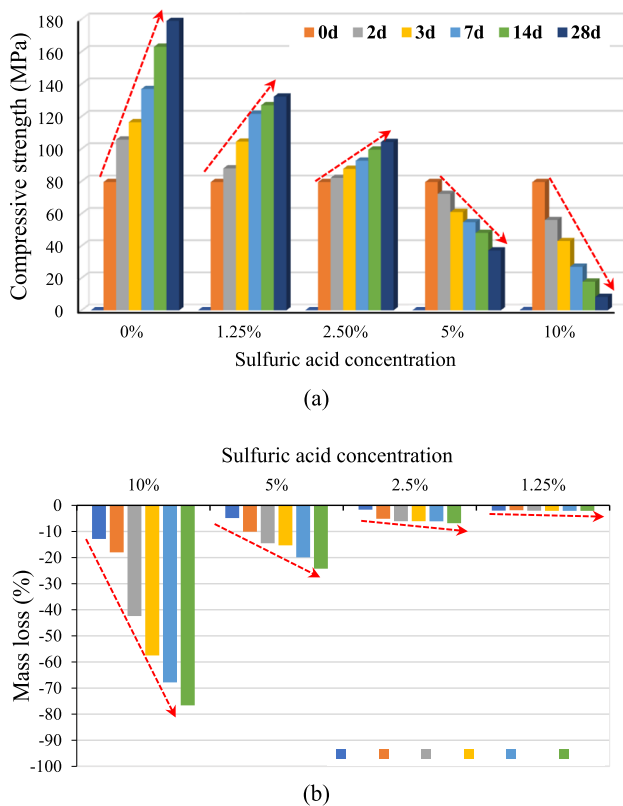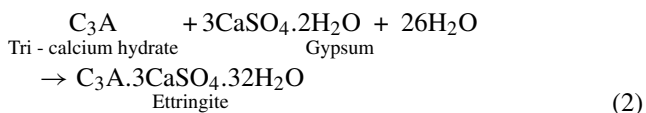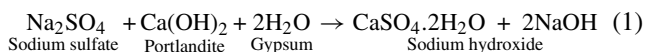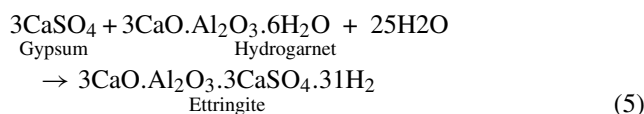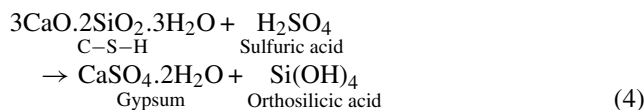
(a)



(b)

**Fig. 14** Effect of **a** different concentrations of sulfuric acid on compressive strength and **b** mass loss of the samples immersed in different sulfuric acid solutions

The use of sodium sulfates to simulate a sulfate attack is a common practice recommended by different standards such as ASTM C1012 and ASTM C452. The percentage of sodium sulfate is usually calculated as the mass of salt per mass of water, as per ASTM standards. The chemical reaction begins with the reaction of sodium sulfate with portlandite in the presence of moisture to form gypsum and sodium hydroxide, as demonstrated in Eq. 1. Then, the formed gypsum attacks the aluminate phase to form ettringite, an expansive mineral, as depicted in Eq. 2. The sulfate attack is highly dependent on concrete permeability, which is determined by the water/cement ratio. Therefore, sulfate attack is expected to be very limited in ultra-high-performance concrete [28–30].

$$\underset{\text{Sodium sulfate}}{Na_2SO_4} + \underset{\text{Portlandite}}{Ca(OH)_2} + 2H_2O \rightarrow \underset{\text{Gypsum}}{CaSO_4.2H_2O} + \underset{\text{Sodium hydroxide}}{2NaOH} \quad (1)$$

$$\underset{\text{Tri - calcium hydrate}}{C_3A} + \underset{\text{Gypsum}}{3CaSO_4.2H_2O} + 26H_2O$$
$$\rightarrow \underset{\text{Ettringite}}{C_3A.3CaSO_4.32H_2O} \quad (2)$$

It has been reported that sulfuric acid attacks on concrete react with cement and aggregates due to its alkaline nature

and carbonaceous aggregates [24, 31–33]. In the reaction with portlandite, gypsum is formed, as illustrated in Eq. 3. As a result of the reaction between sulfuric acid and the hydrated silicate phases, calcium silicate hydrate (C-S-H) decomposes into gypsum and orthosilicic acid (Eq. 4). Expansive ettringite is generated as the final product of the reaction of sulfuric acid with hydrogarnet (tricalcium aluminate hexahydrate, Eq. 5).

$$\underset{\text{Portlandite}}{Ca(OH)_2} + \underset{\text{Sulfuric acid}}{H_2SO_4} \rightarrow \underset{\text{Gypsum}}{CaSO_4.2H_2O} \quad (3)$$

$$\underset{\text{C-S-H}}{3CaO.2SiO_2.3H_2O} + \underset{\text{Sulfuric acid}}{H_2SO_4}$$
$$\rightarrow \underset{\text{Gypsum}}{CaSO_4.2H_2O} + \underset{\text{Orthosilicic acid}}{Si(OH)_4} \quad (4)$$

$$\underset{\text{Gypsum}}{3CaSO_4} + \underset{\text{Hydrogarnet}}{3CaO.Al_2O_3.6H_2O} + 25H2O$$
$$\rightarrow \underset{\text{Ettringite}}{3CaO.Al_2O_3.3CaSO_4.31H_2} \quad (5)$$

As products of the reaction between sulfuric acid and cement, gypsum and orthosilicic acid are not easily washable. The deterioration process is accelerated by ettringite's expansive nature. This type of degradation is evident by the disintegration of the cementitious matrix, while the aggregate grains remain exposed, as demonstrated in Fig. 9 (by the authors).

### 3.3.1 Sulfate Attack

Upon immersion in 10% sodium sulfate and 10% sulfuric acid solutions, the UHPC bars showed no signs of expansion, as shown in Figs. 10, and 11, respectively. This response could be attributed to the elevated impermeability of UHPC samples. This makes it very difficult for sulfate ions to penetrate the sample's surface and initiate the reaction. In order for the expansion to occur, the attacking ions must penetrate the outer surface of the sample [27]. It was expected that the expansion may not occur until this period of testing because of the negligible permeability of the sample surface. Nevertheless, a strong reaction between sulfuric acid and the outer layers of the bar samples resulted in a reduction in their circumference but without significant expansion. The reaction changed the layer into weak gypsum, which detached from the surface while sulfur was formed in solution over time, as shown in Fig. 12. A very low pH (below 1) caused a significant loss of mass in the presence of sulfuric acid, as depicted in Fig. 12 (c), (d), and (g).

In this study, four concentrations of sulfuric acid (1.25, 2.5, 5, and 10%) were prepared and applied to determine the threshold concentration of sulfuric acid that could be tolerated by the UHPC samples. Figure 13 shows that the effect of sulfuric acid decreases with decreasing concentrations as an
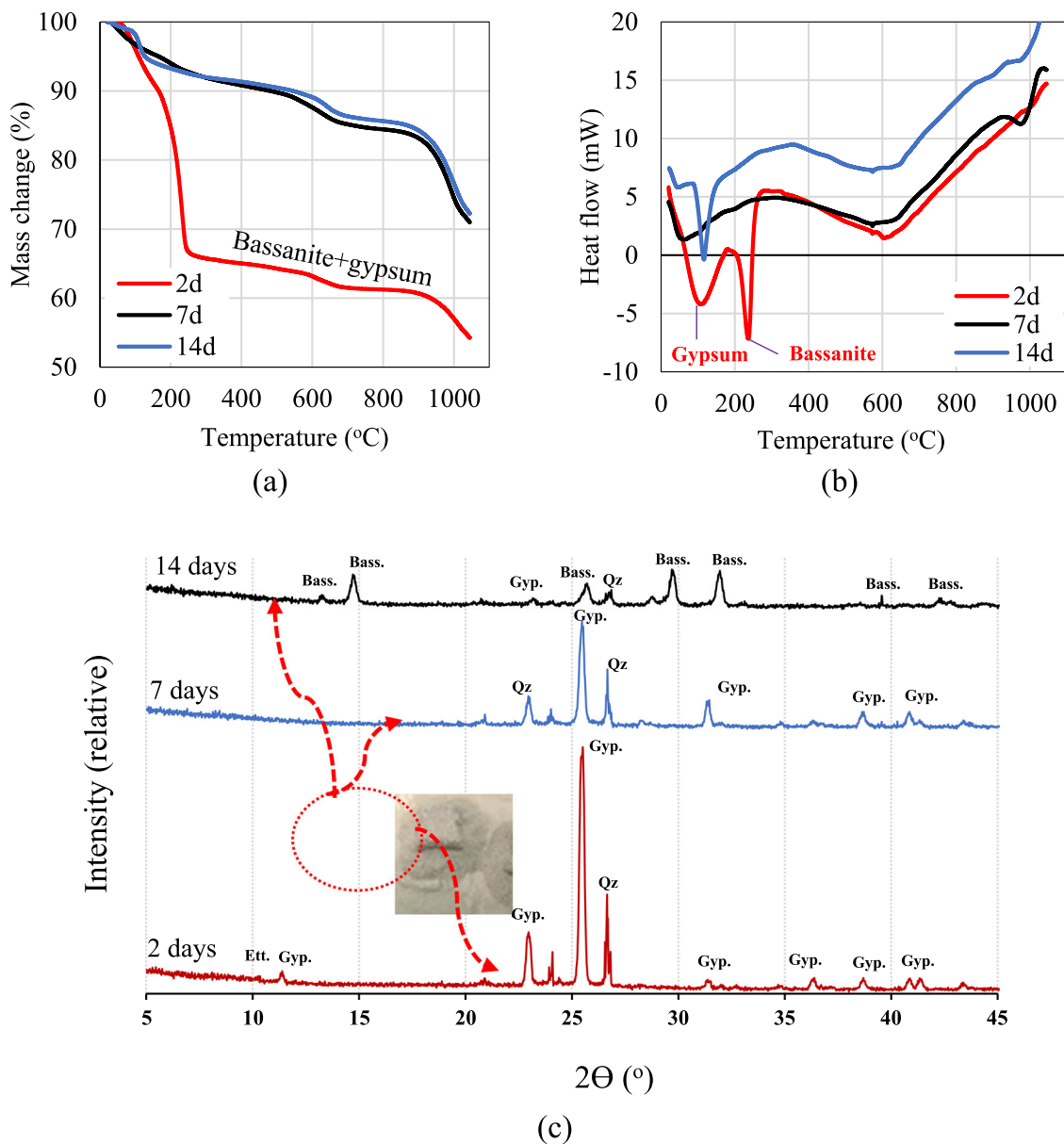
**Fig. 15** Thermal analyses of UHPC samples over time **a** TGA and **b** DSC and **c** XRD analysis of the damaged cementitious matrix of UHPC samples over time

acid-base reaction that is dependent on the concentration of the reactants. Furthermore, Fig. 14 (a) illustrates the effect of sulfuric acid concentrations on compression strength development. While tested UHPC specimens were shown to be able to withstand 1.25% sulfuric acid as opposed to 2.5% sulfuric acid, they still incurred a significant loss due to the weakening of the strength at the surface of contact. At concentrations of 5% and 10%, the compression strength trend inverted (i.e., it decreased with time). The concentration of sulfuric acid has exceeded the critical concentration, which led to a detrimental modification with substantial mass loss.

This loss is due to the formation of the gypsum layer and ettringite as the expansive phase (as demonstrated in Eqns. 1 and 2), which have no bonding capacity and weaken that specimen's strength. Figure 14 (b) displays the results of monitoring the mass loss of the samples. Because of the earlier discussion, the sulfuric acid concentration of 2.5% could be considered a threshold, after which an inflection in the trend takes place.

The results of the thermal and XRD analyses of the damaged cementitious matrices of the UHPC samples are shown in Figs. 15 a and b, respectively. Both figures confirmed that

**Table 5** Monitoring average volume and mass changes of UHPC cube samples in 10% sulfuric acid over time

| Time (min) | 3D (mm) | | | Measured volume (mm$^3$) | Mass (g) | Measured density (g/cm$^3$) | Calculated volume (mm$^3$) |
|---|---|---|---|---|---|---|---|
| | $x$ | $y$ | $z$ | | | | |
| 0 | 25.45 | 25.60 | 26.59 | 17,326.2 | 39.21 | 2.26 | 17,201.4 |
| 1 | 25.35 | 25.54 | 26.51 | 17,165.8 | 39.23 | 2.29 | 17,211.0 |
| 5 | 25.27 | 25.50 | 26.61 | 17,144.9 | 39.23 | 2.29 | 17,208.8 |
| 10 | 25.31 | 25.54 | 26.52 | 17,147.4 | 39.21 | 2.29 | 17,201.4 |
| 20 | 25.32 | 25.55 | 26.60 | 17,205.9 | 39.21 | 2.28 | 17,200.1 |
| 30 | 25.33 | 25.55 | 26.57 | 17,200.1 | 39.17 | 2.28 | 17,182.5 |
| 60 | 25.35 | 25.58 | 26.50 | 17,184.0 | 39.17 | 2.28 | 17,183.8 |
| 120 | 25.29 | 25.60 | 26.53 | 17,178.5 | 39.10 | 2.28 | 17,154.0 |
| 240 | 25.21 | 25.47 | 26.32 | 16,902.2 | 38.65 | 2.29 | 16,954.4 |
| 360 | 25.24 | 25.52 | 26.45 | 17,034.9 | 38.30 | 2.25 | 16,801.3 |
| 480 | 25.02 | 25.51 | 26.45 | 16,879.8 | 38.05 | 2.25 | 16,692.5 |
| 1620 | 24.87 | 25.27 | 26.21 | 16,472.0 | 34.82 | 2.11 | 15,277.6 |
| 1860 | 24.74 | 25.35 | 26.15 | 16,398.1 | 34.22 | 2.09 | 15,011.3 |
| 3000 | 24.04 | 24.92 | 25.66 | 15,378.5 | 31.54 | 2.05 | 13,834.7 |
| 4440 | 23.12 | 24.98 | 23.77 | 13,728.1 | 28.36 | 2.07 | 12,442.3 |
| 5892 | 22.41 | 23.64 | 23.05 | 12,214.7 | 25.33 | 2.07 | 11,113.8 |
| 7332 | 21.70 | 21.34 | 22.73 | 10,527.4 | 22.39 | 2.13 | 9821.4 |
| 8772 | 21.68 | 20.93 | 21.02 | 9539.6 | 19.64 | 2.06 | 8614.5 |
| 10,212 | 20.22 | 21.25 | 19.88 | 8543.4 | 17.13 | 2.01 | 7515.1 |
| 15,972 | 16.52 | 17.57 | 16.40 | 4759.2 | 9.54 | 2.00 | 4185.7 |
| 17,712 | 15.82 | 15.50 | 15.70 | 3847.3 | 7.53 | 1.96 | 3303.1 |
| 19,242 | 15.15 | 16.31 | 15.10 | 3731.2 | 6.82 | 1.83 | 2990.3 |
| 20,727 | 13.71 | 13.84 | 14.07 | 2671.0 | 5.65 | 2.11 | 2477.0 |
| 26,532 | 10.63 | 10.44 | 10.54 | 1169.7 | 2.33 | 1.99 | 1023.5 |
| 29,487 | 9.84 | 8.78 | 8.38 | 724.3 | 1.35 | 1.86 | 591.4 |
| 38,202 | 4.17 | 3.08 | 3.72 | 47.8 | 0.06 | 1.26 | 26.3 |

*Calculated volume is based on the initially measured bulk density = 2.279411 g/cm$^3$

gypsum, bassanite, and ettringite form according to the equations described [Eqs. (3–5)], as depicted by the XRD analysis shown in Fig. 15 (c).

The data collected during the monitoring of the samples' mass and size are shown in Table 5. The monitored samples during testing under visual and microscopic examination are shown in Figs. 16 and 17, respectively.

The measured mass loss and volume change data are presented in Fig. 18 a and b, respectively. The best-fit equation ($y = -0.0052x$) and correlation coefficient ($R^2$) of 0.98

is given in the figure. The x represents the time, while the y represents the percentage of mass loss. Despite the high ratio of solution volume to sample volume, it is evident that the mass loss and volume change have deviated from linearity after more than 10,000 min (i.e., about 7 days). The process has been attributed to the reduced concentration of the acid caused by the chemical interaction. The relationship between the measured volume change and the calculated volume change using mass and density is shown in Fig. 19. The best-fit equation ($y = -0.0054x$) and correlation coefficient ($R^2$) of 0.98 is given in the figure. The x represents the time, while the y represents the percentage of volume change.

**Fig. 16** Demonstration of the tracked change taking place in the UHPC samples



| 1min | 3 hours | 6 hours |

| 24 hours | 3 days | 7 days |

| 12 days | 14 days | 18 days |
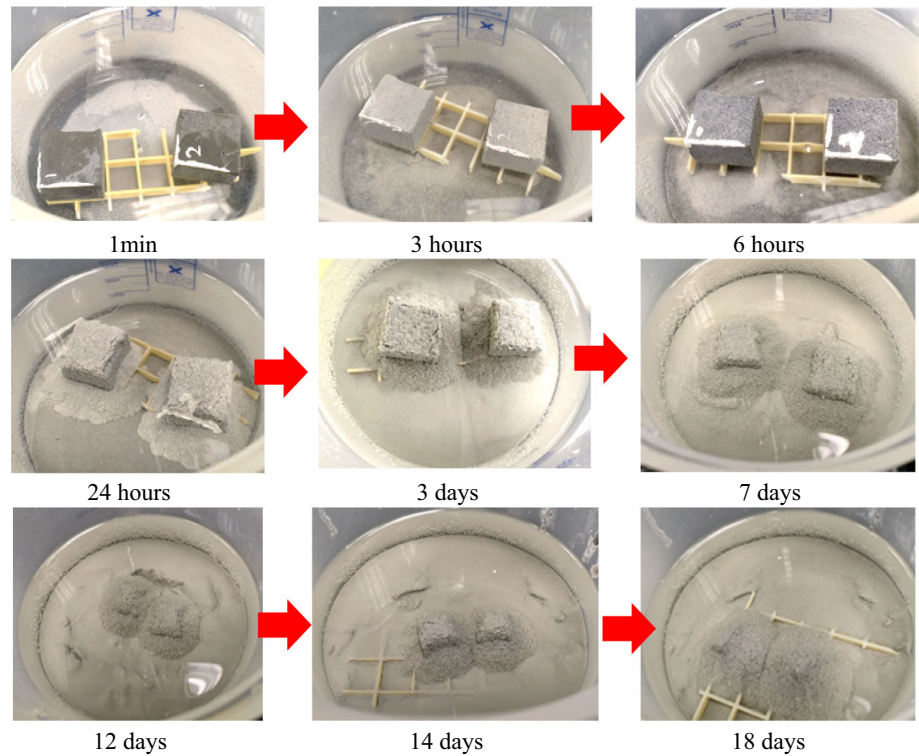
### 3.3.2 Correlating the Mass Loss to the Volumetric Change of the Sample Over Time

In the previous results, it was found that there was a kind of attenuation effect of concentration with the solution's volume to the samples' volume ratio of 10. The aggressive effect decreases as time passes due to the material's consumption of the acid during the reaction. As a result, the solution volume to sample volume ratio must be 30 in order to prevent attenuation in less time. The test setup is shown in Fig. 5. The three axes of the samples were identified to monitor the volume change accurately between the early ages of the samples and their complete damage. Figure 20 shows the typical changes of the samples that take place in the solution and the typical measurement of their size.

## 4 Volume and Mass Change Interpretation

As noted previously, the reduction in size in the three axes ($x$, $y$, and $z$) caused by interaction with 10% sulfuric acid can be tracked by measuring the mass and dimensions of the sample over time in contact with the acid, as shown in Fig. 21. The sample measurement data had been tracked until the damage was complete. Figure 21(a) shows the sample axes, while Fig. 21(b) depicts conversion into smaller sizes, and Fig. 21(c) depicts the typical altered specimen size. The

model's derivation process is shown and described in Fig. 21 and Eqs. 6–9.

Suppose the mass ($m$), density ($\rho$), and volume ($V$) of a cube with a given side length ($x$) can be defined as shown in the following equations:

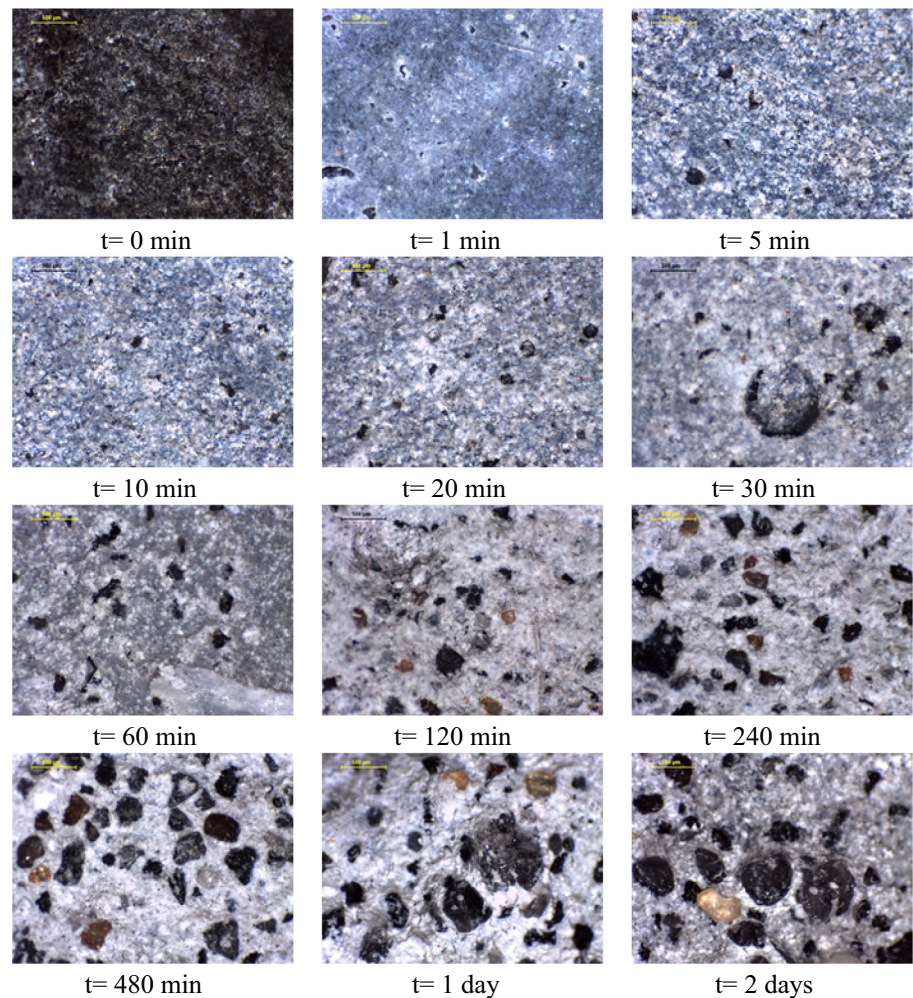$$m = \rho x^3 \tag{6}$$

$$\frac{dm}{dx} = 3\rho x^2 \tag{7}$$

$$dm(g) = 3\rho x^2 dx \tag{8}$$

According to Fig. 22(a), it is evident that the measured volume is slightly higher than the calculated volume based on mass and density. It is obvious that this was a result of protruding aggregates associated with a damaged cementitious matrix, as illustrated in Fig. 22(b).

The measured data before it deviated from linearity was defined, as depicted in Fig. 23. In order to obtain the equation that matches the measured data using Eq. 8, the concentration of sulfuric acid in the solution must also be taken into account. Accordingly, the major equation that best fits the measured data is given by Eq. 9, as shown in Fig. 23

$$\frac{dm}{m} = \left[ \frac{3}{\text{Sulfuric acid concentration}(\%)} \right] \rho x^2 . \frac{dx}{x} \tag{9}$$

**Fig. 17** Microscopic examination of the tested samples in sulfuric acid at different contact times



| | | |
|---|---|---|
| t= 0 min | t= 1 min | t= 5 min |
| t= 10 min | t= 20 min | t= 30 min |
| t= 60 min | t= 120 min | t= 240 min |
| t= 480 min | t= 1 day | t= 2 days |

As the concentration of sulfuric acid declines, the further readings over time for those in Fig. 23 begin to plateau due to the decreased concentration and the reduced degree of aggravation of the acid, as shown in Fig. 24. This deviation from linearity can be avoided by either increasing the volume of the acid solution in this part more than 30 times or by changing the concentration regularly, at least every week.

## 5 Discussion

In comparison with previous studies, it was found that to improve the long-term durability of concrete to chemicals, a modified concrete mix design can be proposed using crumb rubber or another type of concrete, such as geopolymer concrete. In this context, in a previous study conducted to enhance concrete resistivity to chemicals such as chloride and sulfate, the use of crumb rubber was proposed to partially replace fine aggregate up to 30% by weight. Results showed that the presence of 15% crumb rubber can be considered the optimum dosage at which strength and mass loss were at the minimum level compared to the control mix [34]. The use of geopolymer concrete, on the other hand, increased the resistivity to concentrations of 5% sodium chloride, 5% sodium sulfate, and 5% sulfuric acid compared to conventional concrete. However, the use of geopolymer concrete is outside the scope of the current study and will be covered in another work [34]. Therefore, many techniques can be followed to enhance concrete durability in both the short and long term as per the desired properties.

## 6 Conclusions, Recommendations, and Research Prospects

The high cement content of the UHPC mix makes it susceptible to acid attack, despite the presence of fly ash and

**Fig. 18** Monitoring **a** mass and **b** volume changes of UHPC cube samples in 10% sulfuric acid over time



(a)



(b)
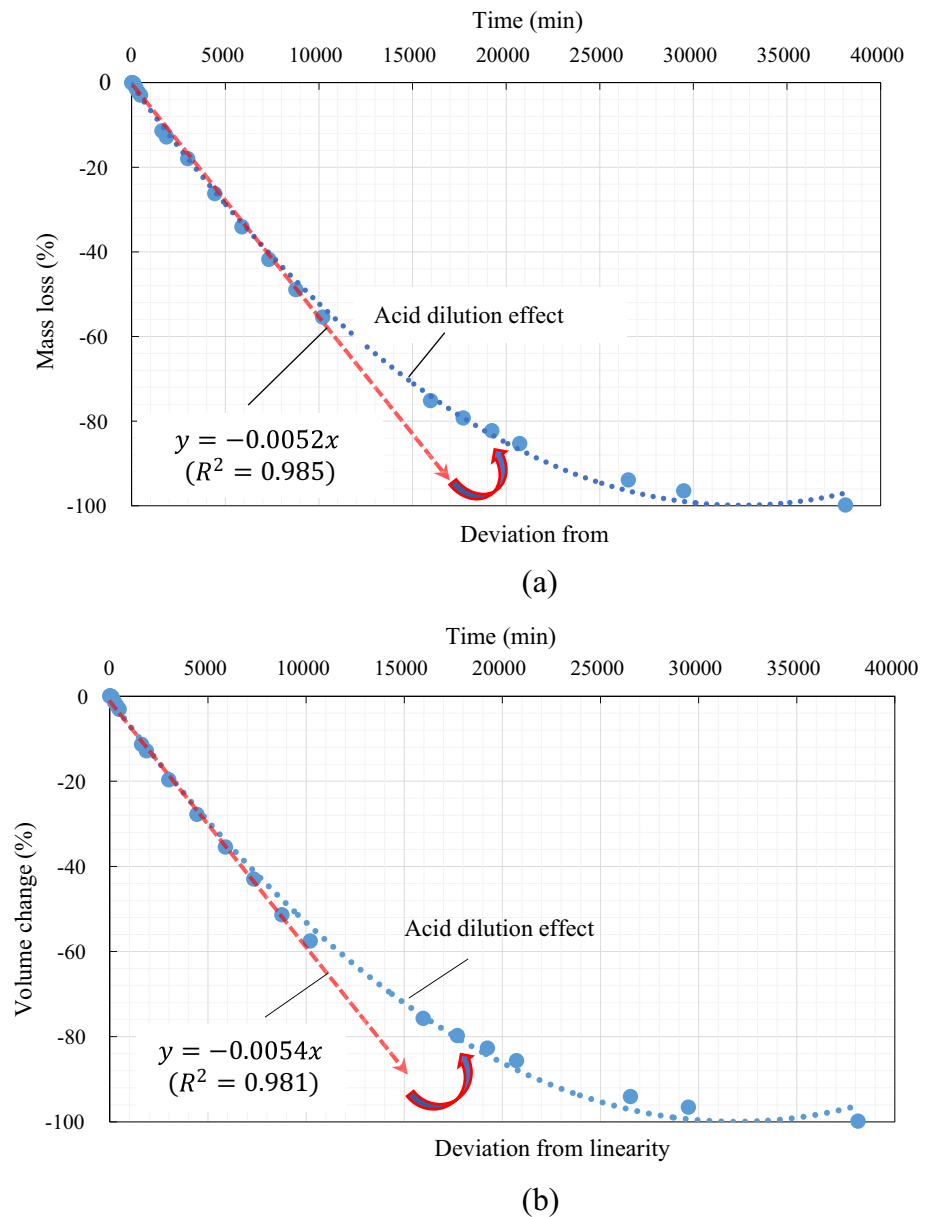
silica fume. An extremely low permeability causes the reaction with sulfate in a high concentration of sodium sulfate to proceed slowly. In conclusion, neither sulfate nor acid attacks caused short-term expansion. In contrast, an acid attack causes visible erosion of the cross-sectional surface area.

The compressive strength of the control and sulfate-cured samples has been gradually increasing. The acid-dissolving reaction of the samples has significantly reduced the size and strength of the acid-cured samples. The optical microscopic analysis of the control and sodium sulfate-cured samples showed that sulfate ions did not attack the surface or cause any obvious damage. However, the formation of gypsum on the surface of a sample cured in sulfuric acid, in addition to the formation of sulfur with time, became noticeable.
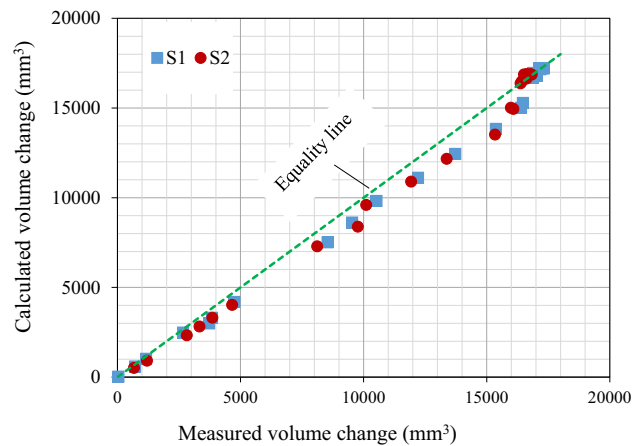


**Fig. 19** Relationship between the measured and calculated volume change of two samples (S1 and S2)

**Fig. 20** Immersion of UHPC samples in 10% sulfuric acid after **a** 1 min, **b** 7 days, and **c** 20 days (complete damage) while typical volume change of the samples during mass loss over time **d** initial reading, **e** 1 day, and **f** 11 days as well as typical measurement of the samples during mass loss over time **g** initial reading, **h** after 11 days, and **i** 18 days
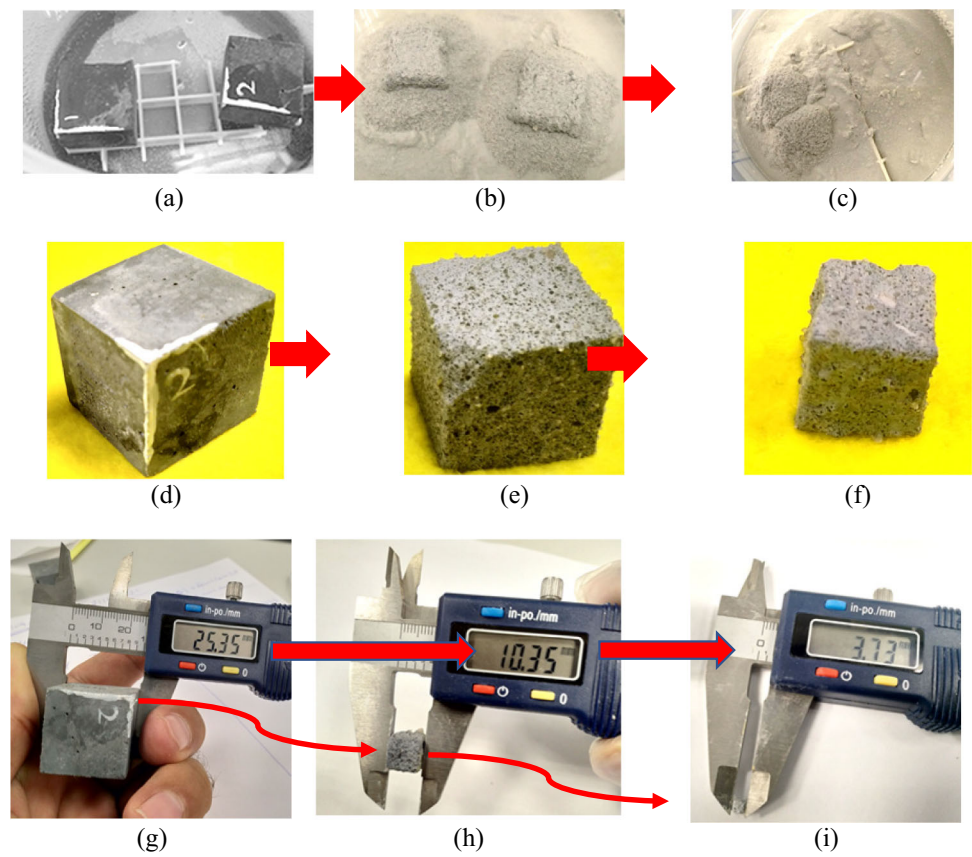


**Fig. 21** Volume change (loss, *dxdydz*) of **a** UHPC cubes **b** over time due to acid attack and **c** typical volume reduction
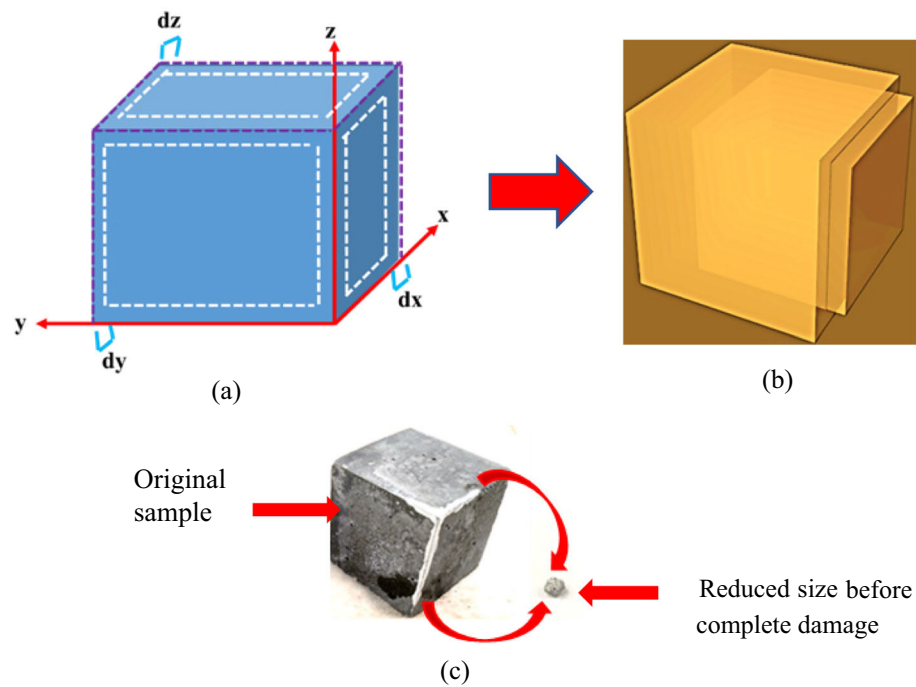
**Fig. 22** Sample's **a** axes measurement and **b** the obvious spacing due to protruded aggregates as a result of damaged cementitious matrix
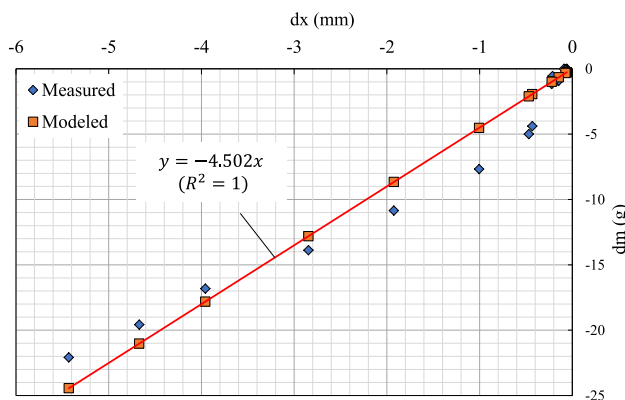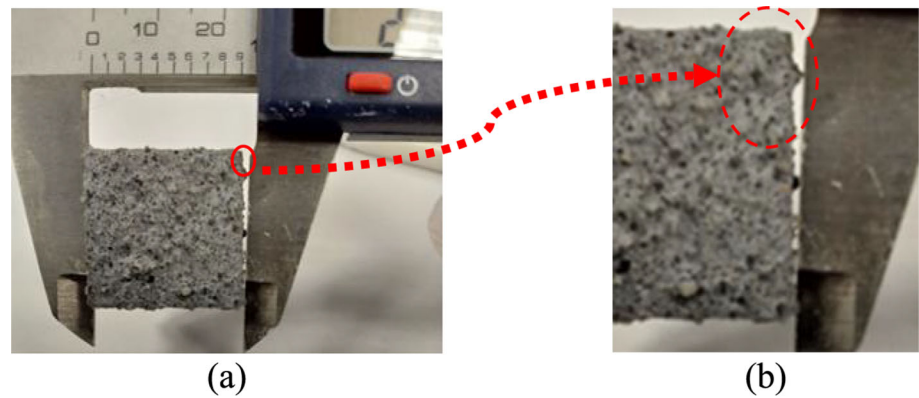


(a)  (b)



**Fig. 23** Measured and modeled data for the relationship between the dimensional variation and mass variation
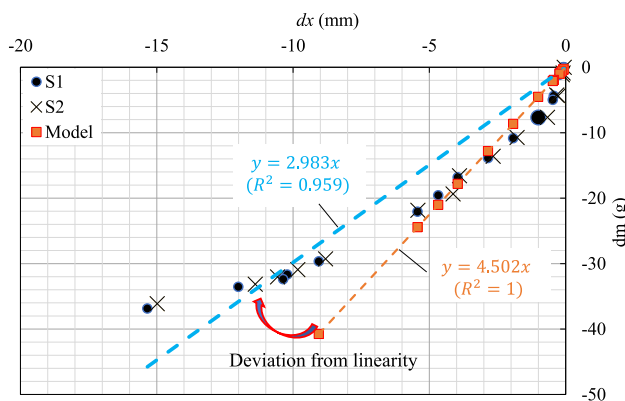


**Fig. 24** Deviation from linearity of UHPC samples (S1 and S2) due to sulfuric acid attenuation over time

Upon immersing the cracked samples with visible micro-steel fibers in 10% sulfuric acid, most of those micro-steel fibers disappeared completely due to corrosion. This damaging reaction highlights the severity of sulfuric acid and its precarious nature with micro-steel fibers. In general, the

mass loss has been varied, ranging between 19 and 21% following a 30-day curing time. In a series of five sulfuric acid concentrations of 0, 1.25, 2.5, 5, and 10%, the threshold concentration that the UHPC samples tolerated was 2.5%.

The formation of gypsum, bassanite, and ettringite due to the reaction of the cementitious matrix with sulfuric acid was confirmed by thermal and XRD examinations of the damaged UHPC samples. For precise modeling of sulfuric acid reactions with UHPC samples, the ideal volume ratio of the solution to the sample was confirmed to be 30 until a certain reaction duration to prevent attenuation effects. Despite the high ratio of solution volume to sample volume, it is clear that the mass loss and volume changes deviated from linearity and occurred after more than 10,000 min, or roughly 7 days.

It is recommended either increase the volume of acid solution over the volume used in this part more than 30 times or alter the concentration weekly to prevent deviations from linearity. It is suggested to investigate other types of minerals and chemical admixtures to evaluate their impact on resistance to acid attack.

## References

1. Aïtcin, P.-C.: High performance concrete. CRC Press, Florida (2011)
2. Almusallam, A.A.; Khan, F.M.; Dulaijan, S.U.; Al-Amoudi, O.S.B.: Effectiveness of surface coatings in improving concrete durability. Cem. Concr. Compos. **25**, 473–481 (2003). https://doi.org/10.1016/S0958-9465(02)00087-2
3. Pfeifer DW, Scali MJ: Concrete sealers for protection of bridge structures (NCHRP report). (1981)
4. Aguiar, J.B.; Camões, A.; Moreira, P.M.: Coatings for concrete protection against aggressive environments. J. Adv. Concr. Technol. **6**, 243–250 (2008). https://doi.org/10.3151/jact.6.243

5. Tahri, W.; Abdollahnejad, Z.; Mendes, J.; Pacheco-Torgal, F.; de Aguiar, J.B.: Cost efficiency and resistance to chemical attack of a fly ash geopolymeric mortar versus epoxy resin and acrylic paint coatings. Eur. J. Environ. Civ. Eng. **21**, 555–571 (2017). https://doi.org/10.1080/19648189.2015.1134674

6. Rahmani, H.; Ramazanianpour, A.A.: Effect of binary cement replacement materials on sulfuric acid resistance of dense concretes. Mag. Concr. Res. **60**, 145–155 (2008). https://doi.org/10.1680/macr.2008.60.2.145

7. Hewayde, E.; Nehdi, M.; Allouche, E.; Nakhla, G.: Effect of mixture design parameters and wetting-drying cycles on resistance of concrete to sulfuric acid attack. J. Mater. Civ. Eng. **19**, 155–163 (2007). https://doi.org/10.1061/(ASCE)0899-1561(2007)19:2(155)

8. Koenig, A., Dehn, F.: Acid resistance of ultra high-performance concrete (UHPC). In: Nanotechnology in construction. pp. 317–323. Springer International Publishing, Cham (2015)

9. Madraszewski, S.; Sielaff, A.M.; Stephan, D.: Acid attack on concrete—damage zones of concrete and kinetics of damage in a simulating laboratory test method for wastewater systems. Constr. Build. Mater. **366**, 130121 (2023). https://doi.org/10.1016/j.conbuildmat.2022.130121

10. Alexander, M.G.; Fourie, C.: Performance of sewer pipe concrete mixtures with portland and calcium aluminate cements subject to mineral and biogenic acid attack. Mater. Struct. **44**, 313–330 (2011). https://doi.org/10.1617/s11527-010-9629-1

11. Senhadji, Y.; Escadeillas, G.; Mouli, M.; Khelafi, H.: Benosman: Influence of natural pozzolan, silica fume and limestone fine on strength, acid resistance and microstructure of mortar. Powder Technol. **254**, 314–323 (2014). https://doi.org/10.1016/j.powtec.2014.01.046

12. He, K.; Yang, H.; Lu, Z.; Jia, F.; Wang, E.; Dong, Q.: Effect of matrix modification on durability of cementitious composites in an acid rain environment. J. Wuhan Univ. Technol.-Mater Sci. Ed. **29**, 498–503 (2014). https://doi.org/10.1007/s11595-014-0947-y

13. Lavigne, M.P.; Bertron, A.; Botanch, C.; Auer, L.; Hernandez-Raquet, G.; Cockx, A.; Foussard, J.-N.; Escadeillas, G.; Paul, E.: Innovative approach to simulating the biodeterioration of industrial cementitious products in sewer environment. Part II: Validation on CAC and BFSC linings. Cem. Concr. Res. **79**, 409–418 (2016). https://doi.org/10.1016/j.cemconres.2015.10.002

14. De Belie, N.; Monteny, J.; Beeldens, A.; Vincke, E.; Van Gemert, D.; Verstraete, W.: Experimental research and prediction of the effect of chemical and biogenic sulfuric acid on different types of commercially produced concrete sewer pipes. Cem. Concr. Res. **34**, 2223–2236 (2004). https://doi.org/10.1016/j.cemconres.2004.02.015

15. Huber, B.; Hilbig, H.; Mago, M.M.; Drewes, J.E.; Müller, E.: Comparative analysis of biogenic and chemical sulfuric acid attack on hardened cement paste using laser ablation-ICP-MS. Cem. Concr. Res. **87**, 14–21 (2016). https://doi.org/10.1016/j.cemconres.2016.05.003

16. Skalny J.; Brown P.: Sulfate attack on concrete. (2002)

17. Shannag, M.J.; Shaia, H.A.: Sulfate resistance of high-performance concrete. Cem. Concr. Compos. **25**, 363–369 (2003). https://doi.org/10.1016/S0958-9465(02)00049-5

18. Tamimi, A.K.: High-performance concrete mix for an optimum protection in acidic conditions. Mater. Struct. **30**, 188–191 (1997). https://doi.org/10.1007/BF02486392

19. Sulfate Resistance of Concrete Containing Mineral Admixtures. ACI Mater. J. 97, (2000). https://doi.org/10.14359/9286

20. American Society for Testing and Materials (ASTM): Standard Specification for Portland Cement (ASTM C150–09). , West Conshohocken, PA, USA (2009)

21. American Society for Testing and Materials (ASTM): Standard Test Method for Density, Relative Density (Specific Gravity), and Absorption of Fine Aggregate (-ASTM C128–01). , West Conshohocken, PA, USA (2017)

22. Khan, M.I.; Fares, G.; Abbas, Y.M.: Cost-performance balance and new image analysis technique for ultra-high performance hybrid nano-based fiber-reinforced concrete. Constr. Build. Mater. **315**, 125753 (2022). https://doi.org/10.1016/j.conbuildmat.2021.125753

23. Khan, M.I.; Fares, G.; Abbas, Y.M.: Behavior of non-shear-strengthened UHPC beams under flexural loading: influence of reinforcement depth. Appl. Sci. **11**, 11168 (2021). https://doi.org/10.3390/app112311168

24. Irico, S.; De Meyst, L.; Qvaeschning, D.; Alonso, M.C.; Villar, K.; De Belie, N.: Severe sulfuric acid attack on self-compacting concrete with granulometrically optimized blast-furnace slag-comparison of different test methods. Materials **13**, 1431 (2020). https://doi.org/10.3390/ma13061431

25. Shariati, M.; Kamyab, H.; Habibi, M.; Ahmadi, S.; Naghipour, M.; Gorjinezhad, F.; Mohammadirad, S.; Aminian, A.: Sulfuric acid resistance of concrete containing coal waste as a partial substitute for fine and coarse aggregates. Fuel **348**, 128311 (2023). https://doi.org/10.1016/j.fuel.2023.128311

26. American Society for Testing and Materials (ASTM): Standard Test Method for Length Change of Hydraulic-Cement Mortars Exposed to a Sulfate Solution (ASTM 1012). , Conshohocken, PA, USA (2013)

27. Vande Voort, T.L.; Suleiman, M.T.; Sritharan, S.: Design and performance verification of UHPC piles for deep foundations. Iowa, USA (2008)

28. Jiang, X.; Mu, S.; Guo, Z.; Liu, G.: Effect of temperature on the physical salt attack of cement mortars under repeated partial immersion in sodium sulfate solution. Materials **15**, 6234 (2022). https://doi.org/10.3390/ma15186234

29. Jiang, X.; Mu, S.; Yang, Z.; Tang, J.; Li, T.: Effect of temperature on durability of cement-based material to physical sulfate attack. Constr. Build. Mater. **266**, 120936 (2021). https://doi.org/10.1016/j.conbuildmat.2020.120936

30. Alyami, M.H.; Alrashidi, R.S.; Mosavi, H.; Almarshoud, M.A.; Riding, K.A.: Potential accelerated test methods for physical sulfate attack on concrete. Constr. Build. Mater. **229**, 116920 (2019). https://doi.org/10.1016/j.conbuildmat.2019.116920

31. ACI Committee 201 (ACI 201.2R-01): Guide to Durable Concrete. , MI, USA. (2008)

32. Bassuoni, M.T.; Nehdi, M.L.: Resistance of self-consolidating concrete to sulfuric acid attack with consecutive pH reduction. Cem. Concr. Res. **37**, 1070–1084 (2007). https://doi.org/10.1016/j.cemconres.2007.04.014

33. Gutberlet, T.; Hilbig, H.; Beddoe, R.E.: Acid attack on hydrated cement—effect of mineral acids on the degradation process. Cem. Concr. Res. **74**, 35–43 (2015). https://doi.org/10.1016/j.cemconres.2015.03.011

34. Kumar, R.; Verma, M.; Dev, N.; Lamba, N.: Influence of chloride and sulfate solution on the long-term durability of modified rubberized concrete. J. Appl. Polym. Sci. (2022). https://doi.org/10.1002/app.52880